

Correlation effects in the tetragonal and collapsed tetragonal phase of CaFe_2As_2

Jean Diehl,* Steffen Backes, Daniel Guterding, Harald O. Jeschke, and Roser Valentí
*Institut für Theoretische Physik, Goethe-Universität Frankfurt,
 Max-von-Laue-Str. 1, 60438 Frankfurt am Main, Germany*
 (Dated: July 25, 2014)

We investigate the role of correlations in the tetragonal and collapsed tetragonal phases of CaFe_2As_2 by performing charge self-consistent DFT+DMFT (density functional theory combined with dynamical mean-field theory) calculations. While the topology of the Fermi surface is basically unaffected by the inclusion of correlation effects, we find important orbital-dependent mass renormalizations which show good agreement with recent angle-resolved photoemission (ARPES) experiments. Moreover, we observe a markedly different behavior of these quantities between the low-pressure tetragonal and the high-pressure collapsed tetragonal phase. We attribute these effects to the increased hybridization between the iron- and arsenic orbitals as one enters the collapsed tetragonal phase.

PACS numbers: 71.15.Mb, 71.18.+y, 71.27.+a, 74.70.Xa

I. INTRODUCTION

The iron-pnictide superconductor CaFe_2As_2 belongs to the so-called 122 family, $A\text{Fe}_2\text{As}_2$ (e.g. $A = \text{Ba}, \text{Sr}, \text{Ca}$) which crystallizes in the ThCr_2Si_2 structure with the $I4/mmm$ space group. CaFe_2As_2 is tetragonal (TET) at room temperature and ambient pressure and undergoes a structural phase transition to an orthorhombic (ORT) phase upon cooling below 170 K.^{1–3} Whereas the tetragonal phase is non-magnetic, the orthorhombic phase shows a stripe-like magnetic order⁴. Upon application of pressure, the appearance of a collapsed tetragonal (CT) phase characterized by a collapse of the c lattice parameter and a volume shrinkage of about 5% with respect to the tetragonal phase was observed.^{3,5} First principles studies have shown that for increasing pressures at low temperature the system goes from the orthorhombic phase directly into the collapsed tetragonal phase at 0.36 GPa, whereas for higher temperatures at high pressure the tetragonal phase is energetically more favorable than the collapsed tetragonal phase.⁶ Moreover, the ORT→CT structural transition coincides with the disappearance of the magnetic moment^{7–10}. Also in BaFe_2As_2 such a collapsed tetragonal phase has been theoretically^{9–11} predicted and experimentally^{12,13} observed, though at much higher pressures of 27 GPa¹³ under hydrostatic pressure conditions.

The appearance of a superconducting phase under pressure was reported in CaFe_2As_2 with a critical temperature of 10 K at 0.69 GPa¹⁴. However, it was recently established that the superconducting region is disjoint from the non-magnetic collapsed tetragonal phase¹⁵ and it is still not entirely clear if superconductivity appears in the orthorhombic phase or in a low temperature tetragonal phase that is stabilized by special non-hydrostatic pressure conditions¹⁶. In order to understand this behaviour, a lot of effort has been devoted

in the last years to investigate the electronic properties of the collapsed tetragonal phase and its main differences compared to the orthorhombic and tetragonal phases. Angle-resolved photoemission (ARPES) measurements for the orthorhombic and tetragonal phases in CaFe_2As_2 at ambient pressure were performed by Liu *et al.*¹⁷, where a two- to three-dimensional transition in the Fermi surface was observed, corresponding to the transition from the tetragonal to the orthorhombic phase at low temperatures. Measurements have also been performed for isostructural materials which are in the collapsed tetragonal phase at ambient pressure: CaFe_2P_2 ¹⁸ and $\text{Ca}(\text{Fe}_{1-x}\text{Rh}_x)_2\text{As}_2$ ¹⁹. In both cases hole pockets around the zone center Γ present in the tetragonal phase disappear in the collapsed tetragonal phase.

Only very recently CaFe_2As_2 samples could be grown in the collapsed tetragonal phase at ambient pressure by introducing internal strain²⁰. In the same work, the authors performed detailed ARPES measurements and found that collapsed tetragonal CaFe_2As_2 shows a similar behavior to CaFe_2P_2 and $\text{Ca}(\text{Fe}_{1-x}\text{Rh}_x)_2\text{As}_2$, namely the disappearance of the hole pockets at the Γ point. While density functional theory (DFT) calculations correctly predict this feature^{10,18,19}, ARPES measurements show a strong band renormalization compared to the DFT calculations.

In order to investigate the origin of this discrepancy, we present in this work an analysis of the electronic structure of tetragonal and collapsed tetragonal phases of CaFe_2As_2 by combining DFT in the GGA approximation with dynamical mean-field theory (GGA+DMFT). This method has been proven to provide a good description of correlation effects in a few families of Fe-based superconductors^{21–26}. While the 122 family has been argued to be less correlated than the so-called 111 or 11 families²³, we will show that also in CaFe_2As_2 correlations are necessary to understand the renormalization of

TABLE I: Lattice parameters for the experimentally measured tetragonal and collapsed tetragonal structure from Ref. 5.

	TET	CT
	$I4/mmm$	$I4/mmm$
T (K)	250	50
p (GPa)	0.0	0.35
a (b) (\AA)	3.8915	3.9792
c (\AA)	11.690	10.6073
z_{As}	0.372	0.3663
V (\AA^3)	177.03	167.96

the bands, where we find a distinct change of orbital-dependent mass enhancements in the transition from the tetragonal to the collapsed tetragonal phase.

II. METHODS

For our fully charge self-consistent GGA+DMFT calculations we consider the tetragonal and collapsed tetragonal structures obtained by neutron diffraction experiments⁵. Lattice parameters and As z position are shown in Table I.

The DFT calculations were performed with the WIEN2K²⁷ implementation of the full-potential linear augmented plane wave (FLAPW) method. As exchange-correlation functional we considered the generalized gradient approximation²⁸ (GGA). The self-consistency cycle employed 726 k -points in the irreducible Brillouin zone, resulting in a $21 \times 21 \times 21$ k mesh in the conventional Brillouin zone, and a $R_{\text{mt}}k_{\text{max}} = 7.0$. For the projection of the Bloch wave functions to the localized Fe $3d$ orbitals we used our own implementation of the method described in Ref. 29,30. The energy window for the projection was chosen to be in the range from -5.9 to 16.0 eV (-6.3 to 16.0 eV) for the tetragonal and collapsed tetragonal structures. We were able to set the lower energy boundary in a gap in the density of states (DOS). The impurity problem was solved with a continuous-time quantum Monte Carlo method in the hybridization expansion³¹ as implemented in the ALPS^{32,33} project. Calculations were done at $\beta = 40 \text{ eV}^{-1}$ with 2×10^6 Monte Carlo sweeps. For the double counting correction the fully localized limit^{34,35} (FLL) scheme was used, although the around mean field³⁶ (AMF) scheme led to comparable results with only slightly less renormalized masses. The interaction parameters are used in the definition of the Slater integrals³⁷ F^k with $U = F^0$ and $J = (F^2 + F^4)/14$. For the onsite correlation we consider a value of $U = 4$ eV and for Hund's rule coupling $J = 0.8$ eV and we analyze the dependency of our results on variations of these parameters. For the analytic continuation of the Monte Carlo data on the imaginary time axis we used a combination of Padé-approximation and a fourth order polyno-

mial fit to the first eight Matsubara frequencies to obtain real frequency data.

In the projection of the Fe $3d$ orbital character, we use a coordinate system which is rotated by 45° around the z -axis with respect to the conventional $I4/mmm$ unit cell so that x - and y -axis point towards neighboring Fe atoms as shown in Fig. 1 (a). In the band structure and Fermi surface plots we choose the usual high symmetry points X , M and Z of the $P4/nmm$ space group to facilitate comparison with the other families of iron pnictides.

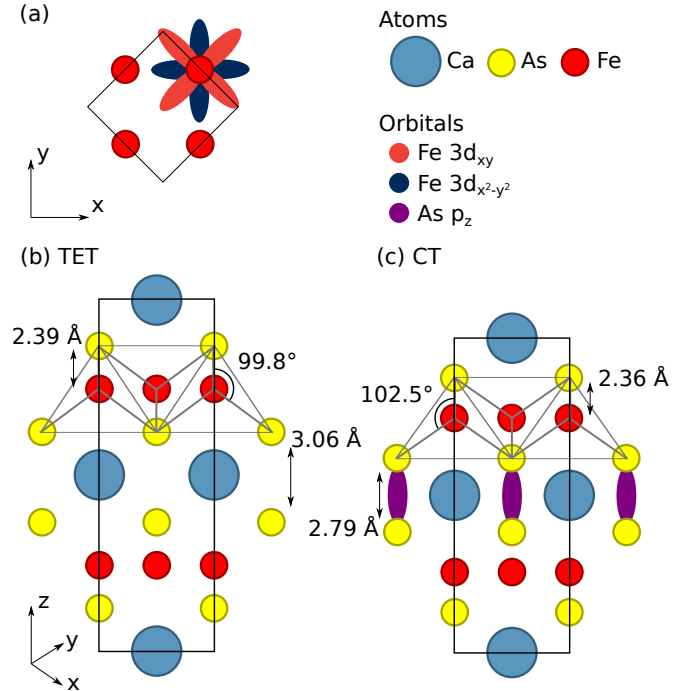


FIG. 1: (Color online) Sketch of (a) the rotated coordinate system with the unit vectors pointing to neighboring iron atoms in the xy -plane. In this projection, Fe $3d_{x^2-y^2}$ orbitals point to neighboring Fe atoms, and Fe $3d_{xy}$ orbitals point towards As atoms. The side-views of the structures in the TET phase in (b) and the CT phase (c) show the collapse along the z -direction, allowing the As atoms to form As dimers in the CT phase when the As-As distance decreases.

III. RESULTS

A. Band structure and spectral function

In Fig. 2 we show a comparison of the DFT (GGA) band structure calculations and the spectral function obtained with GGA+DMFT. We find that correlations mostly renormalize bands in both structures without introducing significant band shifts or altering the topology of the Fermi surface. In the tetragonal phase we observe in both DFT (GGA) as well as GGA+DMFT calculations the presence of three hole bands crossing the Fermi level at the zone center Γ , two electron pockets at

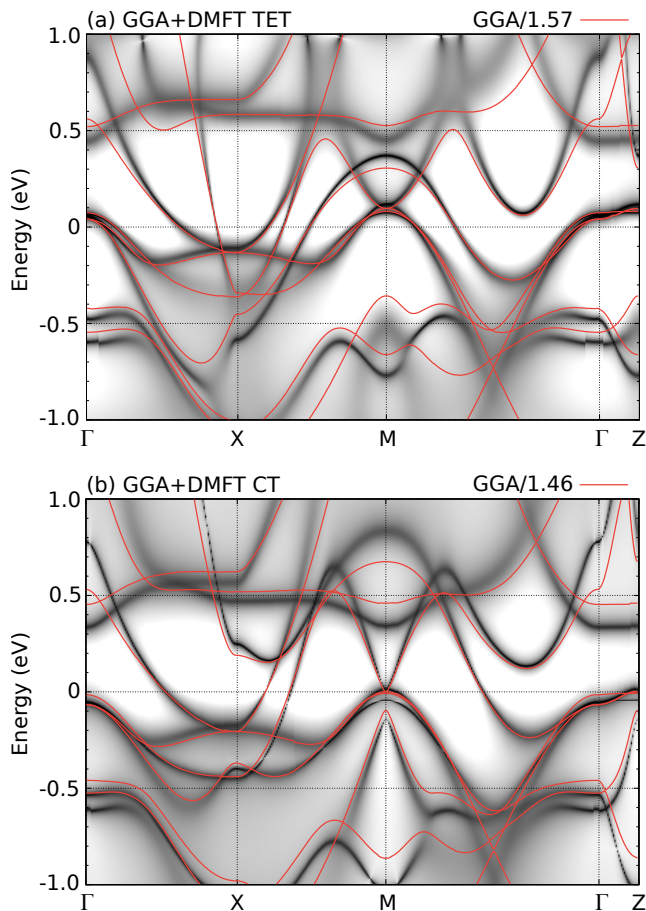


FIG. 2: (Color online) Comparison between GGA band structure (red lines) divided by the orbitally averaged mass enhancements and the momentum resolved spectral function (greyscale in arbitrary units) from GGA+DMFT for (a) the experimental TET structure and (b) the CT structure.

X and three well-defined hole pockets at the zone corner M formed by strongly dispersive hole bands with a large outer pocket and two smaller inner pockets almost identical in size. In the collapsed tetragonal phase the bands at Γ are pushed below the Fermi level in agreement with experiments^{10,18–20}, the inner electron pocket at X is pushed up to positive energies leaving only the slightly enlarged outer electron pocket present. At M the bands forming the inner two hole pockets are pushed onto the Fermi level, leaving two extremely shallow bands of which only one just barely crosses E_F . GGA+DMFT introduces a significant separation between the two bands not observed in the DFT(GGA) calculations. This is a result of the orbital dependent correlations introduced by DMFT.

In Fig. 3 we show the GGA+DMFT results for the same energy range and along the same path in the Brillouin zone as in Ref. 20 in order to allow a better comparison to the ARPES measurements. We find a good agreement between ARPES and our GGA+DMFT calculation in both the tetragonal and the collapsed tetrag-

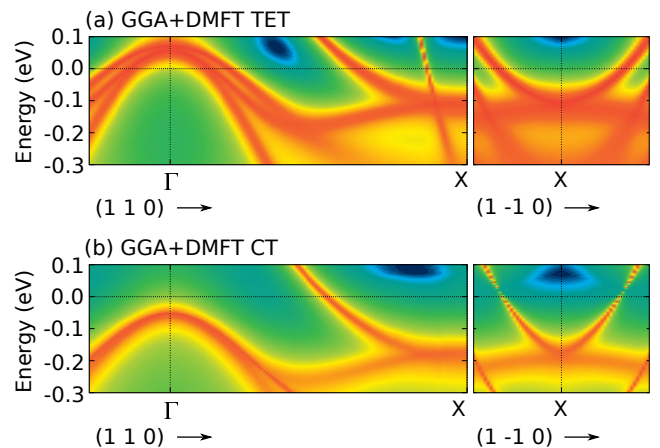


FIG. 3: (Color online) Momentum resolved spectral function around the Fermi level along the same path in the Brillouin zone as in Ref. 20 for (a) the experimental TET structure and (b) the CT structure.

onal phases albeit GGA+DMFT finds a smaller band renormalization than the value extracted from ARPES. Our band renormalizations are about a factor of 1.7 compared to GGA masses while the ARPES measurements report a factor of 5. This suggests that other possible contributions not considered in DMFT may also be important for the description of the electronic behavior of CaFe_2As_2 like non-local correlations and electron-phonon interactions.

The GGA+DMFT Fermi surface for CaFe_2As_2 shows only slight changes compared to DFT(GGA) (see Fig. 4) and agrees reasonably well with ARPES measurements²⁰. The main features of the collapsed tetragonal phase are the disappearance of the hole pockets at Γ as well as a change from a more two-dimensional shape in the tetragonal phase to a three-dimensional shape in the collapsed tetragonal phase (compare the cuts along a plane parallel to the z direction in Figs. 4 (a) and (b)) due to increasing Fe $3d$ -As $4p$ hybridizations.

B. Mass enhancements and sensitivity to interaction parameters

We calculate the effective masses directly from the impurity self-energy via

$$\frac{m^*}{m_{\text{GGA}}} = 1 - \left. \frac{\partial \text{Im}\Sigma(i\omega)}{\partial \omega} \right|_{\omega \rightarrow 0^+}. \quad (1)$$

For the interaction parameters set to $U = 4\text{ eV}$ and $J = 0.8\text{ eV}$ we obtain mass renormalizations between 1.2 and 1.7 as shown in Tab. II for the different orbital characters. Mass renormalizations are strongest for the t_{2g} orbitals Fe $3d_{xy}$ and $3d_{xz/yz}$ in the tetragonal phase while the e_g orbitals $3d_{z^2}$ and $3d_{x^2-y^2}$ are less renormalized both in the tetragonal and collapsed tetragonal phases.

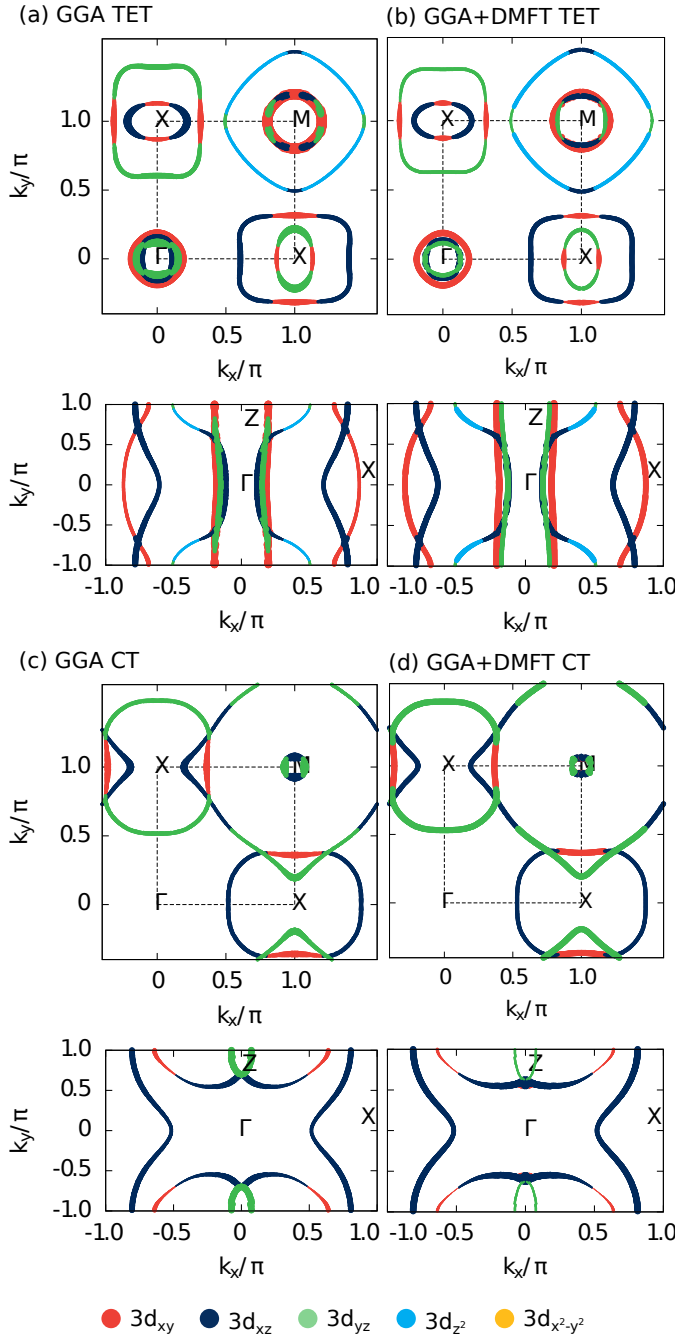


FIG. 4: (Color online) Comparison of the Fermi surface from GGA (left) and GGA+DMFT (right) along a plane at $k_z = 0$ and a vertical cut through the Γ and X point.

As shown in Table II and Fig. 5 we observe a change in the strengths of the mass renormalizations. Interestingly, the iron Fe $3d_{xy}$ orbital undergoes a change from being the most strongly renormalized orbital in the tetragonal phase to the least renormalized orbital in the collapsed tetragonal phase. This can be understood in terms of increased hybridization in the collapsed tetragonal phase. The structural collapse in this phase is assisted by a for-

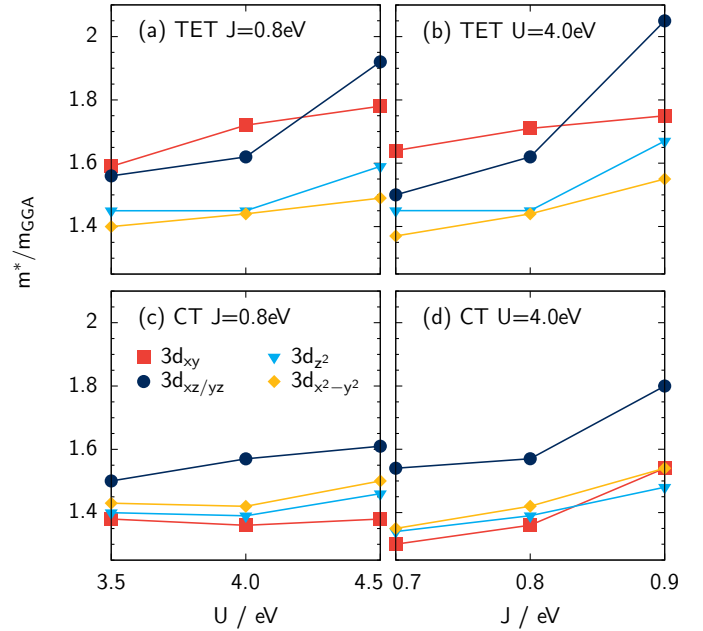


FIG. 5: (Color online) Sensitivity of effective masses m^*/m_{GGA} with respect to changes in the interaction parameters. (a), (c) show variations in U in the tetragonal and the collapsed tetragonal phases respectively, and (b), (d) show variations in J .

TABLE II: Mass renormalizations calculated with GGA+DMFT for the Fe 3d orbitals.

	d_{z^2}	$d_{x^2-y^2}$	d_{xy}	$d_{xz/yz}$
Tetragonal	1.45	1.44	1.72	1.62
Collapsed tetragonal	1.39	1.42	1.36	1.57

mation of As $4p_z$ -As $4p_z$ bonds¹⁰ between the Fe-As layers as shown in Fig. 1 (b) and (c) with a strong bonding-antibonding splitting of the As $4p_z$ bands. The Fe $3d_{xy}$ orbitals, which are pointing in the direction of the As atoms, become less localized in the collapsed tetragonal phase due to increased Fe $3d_{xy}$ -Fe $3d_{xy}$ as well as Fe $3d_{xy}$ -As $4p_x$ and $4p_y$ hybridizations³⁸. This higher degree of delocalization leads to less mass renormalization upon inclusion of correlations.

By varying the interaction parameters U and J we have investigated their influence on the effective masses. The effective masses show stronger dependencies on the Hund's rule coupling J than the Hubbard U as shown in Fig. 5 and as already reported for other members of the iron pnictides^{24,39}. Our results are stable for all values of the chosen interaction parameters and, except for the stronger band renormalization, we observe only very small qualitative changes in the Fermi surface.

In Fig. 6 we show a comparison of the occupation numbers between the GGA and the GGA+DMFT results for the tetragonal and the collapsed tetragonal phases.

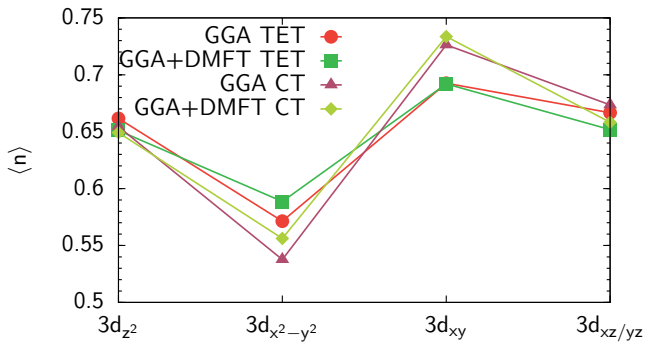


FIG. 6: (Color online) Orbital resolved occupation numbers for the GGA and the GGA+DMFT calculation.

The $3d_{xy}$ and $3d_{xz/yz}$ show the largest occupation with respect to $3d_{z^2}$ and $3d_{x^2-y^2}$ reflecting the crystal field splitting in t_{2g} and e_g orbitals. At the GGA level the transition from tetragonal to collapsed tetragonal phase implies a pronounced increase of charge occupation of the $3d_{xy}$ orbital and to a lesser extent of the $3d_{xz/yz}$, while the occupation for the e_g states decreases. This can also be understood in terms of the change in hybridizations as explained above, where due to the enhanced delocalization of the $3d_{xy}$ electrons in the collapsed tetragonal phase the $3d_{xy}$ orbital becomes less correlated. Regarding the GGA versus GGA+DMFT occupations we observe only little changes and a general trend of electronic charge being shifted from the most correlated orbitals to the less correlated orbitals, as expected, with the total charge on the Fe $3d$ orbitals staying basically identical to the DFT calculation.

Recently, we became aware of the ARPES investigations by Gofryk *et al.*⁴⁰, who reported a distinct increase of the effective masses of the bands around the Γ -point when entering the collapsed tetragonal phase. In order to understand this, we calculated the effective masses m_{GGA}/m_e of the three hole bands around the Γ -point according to the method we described in a previous article⁴¹. In the tetragonal phase we obtained 1.11, 1.62 and $1.71m_e$, while in the CT phase we obtained 1.53, 2.00, $2.89m_e$, with the bands ordered from higher to lower binding energies. Thus, already at the GGA level the trend of increasing renormalization of the bands around Γ in the CT phase is correctly described, albeit the absolute values are lower compared to what was reported from experiment⁴⁰. Therefore, we conclude that the observed increase in band renormalizations from the tetragonal to the CT phase around Γ is mostly due to stronger hybridizations in the collapsed tetragonal phase, as discussed in this section, leading to a shift of the hole bands below the Fermi level. Electronic correlations contribute further only to a minor degree to the effective electronic

mass of the bands around Γ , which we attribute to the fact that CaFe_2As_2 is a weakly to moderately correlated metal.

IV. CONCLUSIONS

We have performed charge self-consistent GGA+DMFT calculations for CaFe_2As_2 in the tetragonal and collapsed tetragonal phases. We observe that while the topology of the Fermi surface in both phases remains nearly unaffected, the orbital-selective mass renormalizations of a factor 1.3 to 1.7 introduced by GGA+DMFT improve the agreement of the calculations with ARPES experiments. The analysis of the influence of the tetragonal to collapsed tetragonal transition on the orbital-dependent effective masses shows that Fe $3d_{xy}$ changes from being the most strongly correlated orbital in the tetragonal phase to being the least correlated one in the collapsed tetragonal phase. We attribute this to the change in hybridization of the Fe $3d$ orbitals in the collapsed tetragonal phase, where due to the decreased distance of the Fe-As layers the hybridization for the Fe $3d_{xy}$ -Fe $3d_{xy}$ as well as Fe $3d_{xy}$ -As $4p_x$ and $4p_y$ orbitals increases, rendering the Fe $3d_{xy}$ less localized and thus less correlated. The orbital occupations confirm this trend and show a higher occupation for the Fe $3d_{xy}$ orbital in the collapsed tetragonal phase.

With these observations we conclude that correlation effects beyond DFT(GGA) as introduced by GGA+DMFT are needed even for weakly correlated pnictides like CaFe_2As_2 in order to understand the orbital-selective mass renormalizations observed in ARPES. However, we also observe that such a description is, nevertheless, still insufficient for explaining the large mass renormalizations observed experimentally. We attribute this discrepancy to possible non-local correlations as well as phononic effects and this will be a subject of future investigations.

During finalization of this manuscript we became aware of another preprint of a DFT+DMFT study of CaFe_2As_2 ⁴², where the authors also find the same trend of reduced renormalization in the CT phase and their results agree, except for minor quantitative differences, with our findings.

Acknowledgments

The authors gratefully acknowledge Milan Tomić, Paul Canfield and Peter Hirschfeld for helpful discussions and the Deutsche Forschungsgemeinschaft for financial support through grant SPP 1458. We thank the centre for scientific computing (CSC, LOEWE-CSC) in Frankfurt for computing facilities.

* jdiehl@itp.uni-frankfurt.de

¹ F. Ronning, T. Klimczuk, E. D. Bauer, H. Volz, and J. D.

- Thompson, J. Phys. Condens. Matter **20**, 322201 (2008).
- ² N. Ni, S. Nandi, A. Kreyssig, A. I. Goldman, E. D. Mun, S. L. Bud'ko, and P. C. Canfield, Phys. Rev. B **78**, 014523 (2008).
 - ³ M. S. Torikachvili, S. L. Bud'ko, N. Ni, and P. C. Canfield, Phys. Rev. Lett. **101**, 057006 (2008).
 - ⁴ S. O. Diallo, V. P. Antropov, T. G. Perring, C. Broholm, J. J. Pulikkotil, N. Ni, S. L. Bud'ko, P. C. Canfield, A. Kreyssig, A. I. Goldman, et al., Phys. Rev. Lett. **102**, 187206 (2009).
 - ⁵ A. Kreyssig, M. Green, Y. Lee, G. Samolyuk, P. Zajdel, J. Lynn, S. Bud'ko, M. Torikachvili, N. Ni, S. Nandi, et al., Phys. Rev. B **78**, 184517 (2008).
 - ⁶ M. Widom and K. Quader, Phys. Rev. B **88**, 045117 (2013).
 - ⁷ T. Yildirim, Phys. Rev. Lett. **101**, 057010 (2008).
 - ⁸ Y.-Z. Zhang, H. C. Kandpal, I. Opahle, H. O. Jeschke, and R. Valentí, Phys. Rev. B **80**, 094530 (2009).
 - ⁹ N. Colonna, G. Profeta, A. Continenza, and S. Massidda, Phys. Rev. B **83**, 094529 (2011).
 - ¹⁰ M. Tomic, R. Valentí, and H. O. Jeschke, Phys. Rev. B **85**, 094105 (2012).
 - ¹¹ S. Backes and H. O. Jeschke, Phys. Rev. B **88**, 075111 (2013).
 - ¹² W. Uhoya, A. Stemshorn, G. Tsoi, Y. K. Vohra, A. S. Sefat, B. C. Sales, K. M. Hope, and S. T. Weir, Phys. Rev. B **82**, 144118 (2010).
 - ¹³ R. Mittal, S. K. Mishra, S. L. Chaplot, S. V. Ovsyannikov, E. Greenberg, D. M. Trots, L. Dubrovinsky, Y. Su, T. Brueckel, S. Matsuishi, et al., Phys. Rev. B **83**, 054503 (2011).
 - ¹⁴ T. Park, E. Park, H. Lee, T. Klimczuk, E. D. Bauer, F. Ronning, and J. D. Thompson, J. Phys. Condens. Matter **20**, 322204 (2008).
 - ¹⁵ J. H. Soh, G. S. Tucker, D. K. Pratt, D. L. Abernathy, M. B. Stone, S. Ran, S. L. Bud'ko, P. C. Canfield, A. Kreyssig, R. J. McQueeney, et al., Phys. Rev. Lett. **111**, 227002 (2013).
 - ¹⁶ K. Prokeš, A. Kreyssig, B. Ouladdiaf, D. K. Pratt, N. Ni, S. L. Bud'ko, P. C. Canfield, R. J. McQueeney, D. N. Argyriou, and A. I. Goldman, Phys. Rev. B **81**, 180506 (2010).
 - ¹⁷ C. Liu, T. Kondo, N. Ni, A. A. Palczewski, A. Bostwick, G. Samolyuk, R. Khasanov, M. Shi, E. Rotenberg, S. Bud'ko, et al., Phys. Rev. Lett. **102**, 167004 (2009).
 - ¹⁸ A. I. Coldea, C. M. J. Andrew, J. G. Analytis, R. D. McDonald, A. F. Bangura, J. H. Chu, I. R. Fisher, and A. Carington, Phys. Rev. Lett. **103**, 026404 (2009).
 - ¹⁹ K. Tsubota, T. Wakita, H. Nagao, C. Hiramatsu, T. Ishiga, M. Sunagawa, K. Ono, H. Kumigashira, M. Danura, K. Kudo, et al., Journal of the Physical Society of Japan **82**, 073705 (2013).
 - ²⁰ R. S. Dhaka, R. Jiang, S. Ran, S. L. Bud'ko, P. C. Canfield, B. N. Harmon, A. Kaminski, M. Tomić, R. Valentí, and Y. Lee, Phys. Rev. B **89**, 020511 (2014).
 - ²¹ M. Aichhorn, S. Biermann, T. Miyake, A. Georges, and M. Imada, Phys. Rev. B **82**, 064504 (2010).
 - ²² M. Aichhorn, L. Pourovskii, and A. Georges, Phys. Rev. B **84**, 054529 (2011).
 - ²³ Z. P. Yin, K. Haule, and G. Kotliar, Nat. Mater. **10**, 932 (2011).
 - ²⁴ J. Ferber, K. Foyevtsova, R. Valentí, and H. O. Jeschke, Phys. Rev. B **85**, 094505 (2012).
 - ²⁵ J. Ferber, H. O. Jeschke, and R. Valentí, Phys. Rev. Lett. **109**, 236403 (2012).
 - ²⁶ P. Werner, M. Casula, T. Miyake, F. Aryasetiawan, A. J. Millis, and S. Biermann, Nat. Phys. **8**, 331 (2012).
 - ²⁷ P. Blaha, K. Schwarz, G. K. H. Madsen, D. Kvasnicka, and J. Luitz, *An Augmented Plane Wave Plus Local Orbitals Program for Calculating Crystal Properties*, vol. 1 (2001).
 - ²⁸ J. P. Perdew, K. Burke, and Y. Wang, Phys. Rev. B **54**, 16533 (1996).
 - ²⁹ M. Aichhorn, L. Pourovskii, V. Vildosola, M. Ferrero, O. Parcollet, T. Miyake, A. Georges, and S. Biermann, Phys. Rev. B **80**, 085101 (2009).
 - ³⁰ J. Ferber, K. Foyevtsova, H. O. Jeschke, and R. Valentí, Phys. Rev. B **89**, 205106 (2014).
 - ³¹ P. Werner, A. Comanac, L. de' Medici, M. Troyer, and A. J. Millis, Phys. Rev. Lett. **97**, 076405 (2006).
 - ³² B. Bauer, L. D. Carr, H. G. Evertz, A. Feiguin, J. Freire, S. Fuchs, L. Gamper, J. Gukelberger, E. Gull, S. Guertler, et al., J. Stat. Mech. Theory Exp. **2011**, P05001 (2011).
 - ³³ E. Gull, P. Werner, S. Fuchs, B. Surer, T. Pruschke, and M. Troyer, Comput. Phys. Commun. **182**, 1078 (2011).
 - ³⁴ V. I. Anisimov, I. V. Solovyev, M. A. Korotin, M. T. Czyzyk, and G. A. Sawatzky, Phys. Rev. B **48**, 16929 (1993).
 - ³⁵ S. L. Dudarev, G. A. Botton, S. Y. Savrasov, C. J. Humphreys and A. P. Sutton, Phys. Rev. B **57**, 1505 (1998).
 - ³⁶ M. T. Czyzyk and G. A. Sawatzky, Phys. Rev. B **49**, 14211 (1994).
 - ³⁷ A. I. Liechtenstein, V. I. Anisimov, and J. Zaanen, Phys. Rev. B **52**, 5467 (1995).
 - ³⁸ We have confirmed this trend by a tight-binding analysis of the bandstructure in the tetragonal and collapsed tetragonal phases (Milan Tomić, private communication).
 - ³⁹ K. Haule and G. Kotliar, New Journal of Physics **11**, 025021 (2009).
 - ⁴⁰ K. Gofryk, B. Saparov, T. Durakiewicz, A. Chikina, S. Danzenbächer, D. V. Vyalikh, M. J. Graf and A. S. Sefat, Phys. Rev. Lett. **112**, 186401 (2014).
 - ⁴¹ S. Backes, D. Guterding, H. O. Jeschke and R. Valentí, arXiv:1403.6993 (2014).
 - ⁴² S. Mandal, R. E. Cohen and K. Haule, arXiv:1407.4876 (2014).